M-CSF inhibition selectively targets pathological angiogenesis and lymphangiogenesis

Yoshiaki Kubota,[1] Keiyo Takubo,[1] Takatsune Shimizu,[2] Hiroaki Ohno,[4] Kazuo Kishi,[3] Masabumi Shibuya,[5] Hideyuki Saya,[2] and Toshio Suda[1]

[1]Department of Cell Differentiation, The Sakaguchi Laboratory, [2]Division of Gene Regulation, Institute for Advanced Medical Research, and [3]Department of Plastic Surgery, School of Medicine, Keio University, Shinjuku-ku, Tokyo 160-8582, Japan
[4]Pharmacological Research Laboratories, Research Division, Kyowa Hakko Kirin Co., LTD., Gunma 370-1295, Japan
[5]Department of Molecular Oncology, Graduate School of Medicine and Dentistry, Tokyo Medical and Dental University, Bunkyo-ku, Tokyo 113-8519, Japan

Antiangiogenic therapy for the treatment of cancer and other neovascular diseases is desired to be selective for pathological angiogenesis and lymphangiogenesis. Macrophage colony-stimulating factor (M-CSF), a cytokine required for the differentiation of monocyte lineage cells, promotes the formation of high-density vessel networks in tumors and therefore possesses therapeutic potential as an M-CSF inhibitor. However, the physiological role of M-CSF in vascular and lymphatic development, as well as the precise mechanisms underlying the antiangiogenic effects of M-CSF inhibition, remains unclear. Moreover, therapeutic potential of M-CSF inhibition in other neovascular diseases has not yet been evaluated. We used *osteopetrotic* (*op/op*) mice to demonstrate that M-CSF deficiency reduces the abundance of LYVE-1$^+$ and LYVE1$^-$ macrophages, resulting in defects in vascular and lymphatic development. In ischemic retinopathy, M-CSF was required for pathological neovascularization but was not required for the recovery of normal vasculature. In mouse osteosarcoma, M-CSF inhibition effectively suppressed tumor angiogenesis and lymphangiogenesis, and it disorganized extracellular matrices. In contrast to VEGF blockade, interruption of M-CSF inhibition did not promote rapid vascular regrowth. Continuous M-CSF inhibition did not affect healthy vascular and lymphatic systems outside tumors. These results suggest that M-CSF–targeted therapy is an ideal strategy for treating ocular neovascular diseases and cancer.

CORRESPONDENCE
Yoshiaki Kubota:
ykubo33@sc.itc.keio.ac.jp
OR
Toshio Suda:
sudato@sc.itc.keio.ac.jp

Abbreviations used: BW, body weight; ECM, extracellular matrix; IHC, immunohistochemistry; ISH, in situ hybridization; M-CSF, macrophage CSF; MMP, matrix metalloproteinase; MNC, mononuclear cell; NVT, neovascular tuft; OIR, oxygen-induced retinopathy; *op/op*, *osteopetrotic*; VEGF, vascular endothelial growth factor.

Pathological angiogenesis is a hallmark of cancer and various inflammatory conditions including ocular neovascular diseases (1, 2). Recent studies have led to the discovery of a growing number of antiangiogenic molecules, some of which are already being evaluated in clinical trials (1, 2). The most established approach for limiting pathological angiogenesis involves blockade of the vascular endothelial growth factor (VEGF) pathway (3–5); however, several studies have shown that VEGF blockade damages healthy vessels and results in toxic side effects (6, 7) and that interrupting the VEGF blockade induces rapid vascular regrowth in tumors (8). Clinical trials involving patients with neovascular age-related macular degeneration have shown that VEGF blockade has limited effectiveness in some patients (5). Therefore, several groups have explored other targets that could potentially be combined with VEGF blockade (9–11). In particular, tumor-associated hematopoietic cells are thought to be a promising therapeutic target, especially neutralizing Bv8, which promotes both tissue-specific angiogenesis and hematopoietic cell mobilization (10).

Macrophage CSF (M-CSF) (12) is a cytokine required for the differentiation of monocyte lineage cells (e.g., tissue macrophages, osteoclasts, and microglia) during development (13, 14). Although greatly reduced numbers of monocyte lineage cells are present in *osteopetrotic* (*op/op*) mutant mice (i.e., mice that possess a mutant *csf-1* gene encoding M-CSF) (13), the potential

The Rockefeller University Press $30.00
J. Exp. Med. Vol. 206 No. 5 1089-1102
www.jem.org/cgi/doi/10.1084/jem.20081605

The Journal of Experimental Medicine

effects on angiogenesis and lymphangiogenesis have not been evaluated. Recent studies suggest that M-CSF plays a key role in the formation of high-density vessel networks and acts as an "angiogenic switch" in a mouse model of mammary tumors (15, 16). The inhibition of M-CSF by antisense oligonucleotides, small interfering RNAs, or blocking antibodies suppresses the growth of human mammary tumor xenografts in mice (17, 18). Clodronate liposome, a reagent for depleting macrophages, also inhibits tumor growth (19). However, the mechanisms underlying the role of M-CSF in tumor progression, particularly with regards to tumor lymphangiogenesis and tumor selectivity, have not been fully dissected.

Osteosarcoma, the most common primary bone tumor, is defined as a malignant tumor derived from mesenchymal or stromal cells with highly metastatic capacities, particularly in the lung and liver (20). Multimodal treatment, often consisting of aggressive chemotherapy combined with radical surgical resection (e.g., limb amputation), has traditionally been the mainstay of osteosarcoma management; however, the prognosis of osteosarcoma patients has not improved significantly in recent years (20). Lack of an appropriate animal model for human osteosarcoma has hampered the development of an effective antiosteosarcoma therapy.

In this study, we used *op/op* mice to demonstrate that M-CSF contributes to both vascular and lymphatic development. Furthermore, our data show that M-CSF is required for retinal pathological neovascularization but not for the maintenance of stable adult vasculature or lymphatics. Using a newly established mouse model of osteosarcoma, we show that M-CSF inhibition selectively suppresses tumor angiogenesis and lymphangiogenesis. In contrast to VEGF blockade, the interruption of M-CSF inhibition does not promote rapid tumor regrowth. These findings indicate that M-CSF–targeted therapy is an ideal strategy for the treatment of ocular neovascular diseases and cancer.

RESULTS

M-CSF contributes to developmental vascular remodeling but not to maintenance of adult vasculature

Postnatal retinal vascular development, a widely used model for studying sprouting angiogenesis, can be used to study pathological angiogenesis (e.g., the formation of blood vessels in tumors) (21, 22). We first characterized macrophages in a retinal angiogenesis model. Macrophages stained with Mac-1 were found in avascular and vascularized areas and were readily distinguished from desmin-stained pericytes (Fig. 1 A). Active vascular remodeling takes place in capillary areas during the pruning of vascular capillary components (23). Macrophages in these areas had large expanded cytoplasms and contained vesicles positive for PECAM-1 (Fig. 1 B) in contrast to the lean bodies observed in arterial areas (Fig. 1 C). Immunostaining of laminin revealed the presence of basal lamina between macrophages and pericytes (Fig. 1 D). We then examined several angiogenic factors and were unable to detect VEGF in macrophages via in situ hybridization (ISH; Fig. 1 E). Furthermore, abundant matrix metalloproteinase (MMP) 9 (Fig. 1 F) and MMP-2 (not depicted) expression was detected on the cell surfaces of macrophages. Both of these MMPs are macrophage-derived proteases that work with modulating extracellular matrix (ECM) proteins, such as fibronectin, to remodel vascular structures (24). Macrophages contribute to programmed cell death in temporary hyaloid vessels via Wnt7b (25); however, their role in the formation of retinal vascular plexus has not yet been clarified. Therefore, we examined the role of M-CSF in developmental angiogenesis by examining the retinal vascular structures of *op/op* mice, which lack macrophages stained with Mac-1, F4/80, CD45, or isolectin (Fig. 1, G and H). By postnatal day (P) 2, branching was reduced in the vascular plexus of the *op/op* retina (Fig. 2, A, B, and K), but the numbers of endothelial tip cells and filopodia (which are regulated by VEGF [26]) were comparable to those in wild-type mice (Fig. 2 J). Vascular defects in the *op/op* retina were also detected on P4, as shown by significantly reduced branching and insufficient arterial-venous patterning (Fig. 2, C, D, and K). The reduced branching observed in *op/op* mice recovered as development progressed (Fig. 2 K and Fig. S1, A and B). 3 mo after birth, the vasculature of *op/op* retinas was comparable to that in +/+ retinas (Fig. S1, C and D). We then investigated the mechanisms underlying vascular impairment in the *op/op* retina. Although VEGF expression remained the same (Fig. 2, E and F), the expression of MMP-2 and MMP-9 (Fig. 2 I) was decreased in the *op/op* retina. Presumably because of this decreased proteinase activity, *op/op* retina showed disordered fibronectin architecture (Fig. 2, G and H). To examine the function of M-CSF in the postnatal developing retina, wild-type mice were systemically treated with a small molecule tyrosine kinase inhibitor specific for c-fms (Ki20227) (27) or intraocularly injected with anti–c-fms neutralizing antibodies (AFS98) (28) during the postnatal stage. Both treatments significantly reduced branching by P4, but the number of endothelial tip cells was comparable to that in control mice (i.e., mice treated with vehicle alone) (Fig. 2, L–P). The reduction rate for branching points was greater in response to M-CSF inhibition than in response to M-CSF deficiency, suggesting that some form of compensation occurs in the postnatal *op/op* retina. When retinas were treated with Ki20227/anti–c-fms antibodies, macrophages decreased in number and exhibited insufficient stellate morphology (Fig. 2, L–P). Thus, these results suggest that M-CSF contributes to developmental vascular remodeling independently of VEGF but does not contribute to the maintenance of adult vasculature.

M-CSF is required for pathological neovascularization but not for recovery of normal vasculature in oxygen-induced retinopathy (OIR)

Although normalized vasculature in the later stage of *op/op* mice suggests that M-CSF is not required for the maintenance of stable adult vasculature, we suspected that M-CSF might be critical for the induction of pathological neovascularization. The OIR model (29) is a widely used system to examine ocular neovascularization, a condition which resembles proliferative diabetic retinopathy in humans (30). In this model, the

central area of established vasculature is obliterated by hyperoxic insult, creating an ischemic area. After mice are returned to room air, revascularization occurs and the normal vasculature is recovered, although some vessels (i.e., neovascular tufts [NVTs]) proliferate abnormally toward the vitreous body (Fig. 3 A). Increased expression of *csf-1*, *vegf-a*, and the c-fms receptor (*csfr-1*) was observed during neovascularization in the OIR model (Fig. 3, B–D). In addition, *csfr-1* expression was higher in FACS-sorted Mac1$^+$ cells than in Mac1$^-$ cells (Fig. 3 E), suggesting that *csfr-1* is specific to macrophages. These data also indicate that *csfr-1* expression in tissues largely reflects the number of macrophages. There was no significant difference in the vaso-obliterated areas of wild-type and *op/op* retina on P11 in the OIR model (Fig. S2, A, B, E, F, and I), suggesting that vascular resistance to hyper oxygen insult was not altered in *op/op* retina. Similarly, Ki20227 treatment did not alter vascular resistance to hyper oxygen insult (Fig. S2, C, D, G, H, and J). On P16, the *op/op* retina exhibited a dramatic decrease in NVTs but an increase in physiological revascularization (Fig. 3, F–I and V). To confirm the role of M-CSF in neovascularization, wild-type mice were systemically treated with Ki20227 or intraocularly injected with anti–c-fms neutralizing antibodies during neovascularization. Both avascular and NVT areas dramatically decreased in response to these treatments, relative to mice treated with vehicle or control IgG (Fig. 3, J–O and V). The number of macrophages surrounding NVT areas dramatically decreased in mice treated with Ki20227/anti–c-fms antibodies, as well as in *op/op* mice (Fig. 3, R–U [quantification not depicted]). Retinas in MMP-9$^{-/-}$ mice exhibited significantly fewer NVTs but increased physiological revascularization (unpublished data). In contrast, treatment with SU1498, a potent and selective inhibitor of VEGFR2, nonselectively suppressed both pathological and physiological angiogenesis (Fig. 3, P, Q, and V). Collectively, these data suggest that targeting macrophage/ECM-related molecules selectively inhibits pathological neovascularization but does not affect the recovery of normal vasculature in the OIR model.

M-CSF contributes to postnatal lymphatic development

Macrophages are thought to play important roles in lymphangiogenesis, particularly in macrophage subpopulations that express LYVE-1, a marker of lymphatics. In these subpopulations,

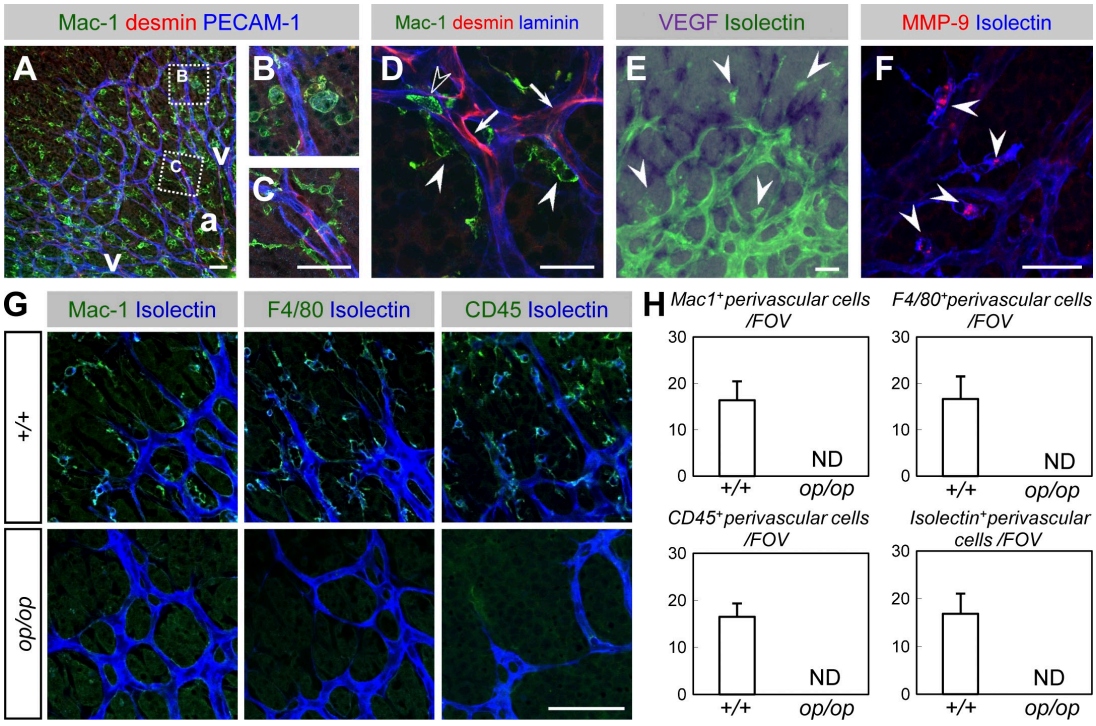

Figure 1. Characterization of macrophages in the developing retina. (A–C) Triple immunohistochemistry (IHC) of Mac-1 (green), desmin (red), and PECAM-1 (blue) within the P4 retina (representative images of three independent experiments). Macrophages in the venous/capillary (v) area possessed largely expanded cytoplasms and contained vesicles positive for PECAM-1 (B) in contrast to their lean bodies in the arterial area (a; C). (D) Triple IHC of Mac-1 (green), desmin (red), and laminin (blue; a representative image of three independent experiments). Macrophages (closed arrowheads) were identified in the perivascular space outside the basement membrane, whereas pericytes (arrows) and circulating monocytes (open arrowheads) were identified inside the basement membrane. (E) An ISH analysis of VEGF (purple) combined with isolectin B4 staining (green) of P4 (a representative image of six independent experiments). Macrophages (arrowheads) did not express VEGF, whereas astrocytes abundantly expressed VEGF. (F) An IHC analysis of MMP-9 (red) combined with isolectin B4 staining (blue; representative images of three independent experiments). MMP-9 was abundantly expressed in macrophages (arrowheads). (G) Double IHC of isolectin B4 (blue) and Mac-1, CD45, or F4/80 (green, as indicated) at P4 (representative images of eight independent experiments). Note that perivascular cells stained with Mac-1, CD45, F4/80, or isolectin were all identical and were absent from *op/op* mice. (H) Quantification of perivascular cells (mean ± SD) stained with Mac-1, CD45, or F4/80 (n = 8). Bars, 50 µm.

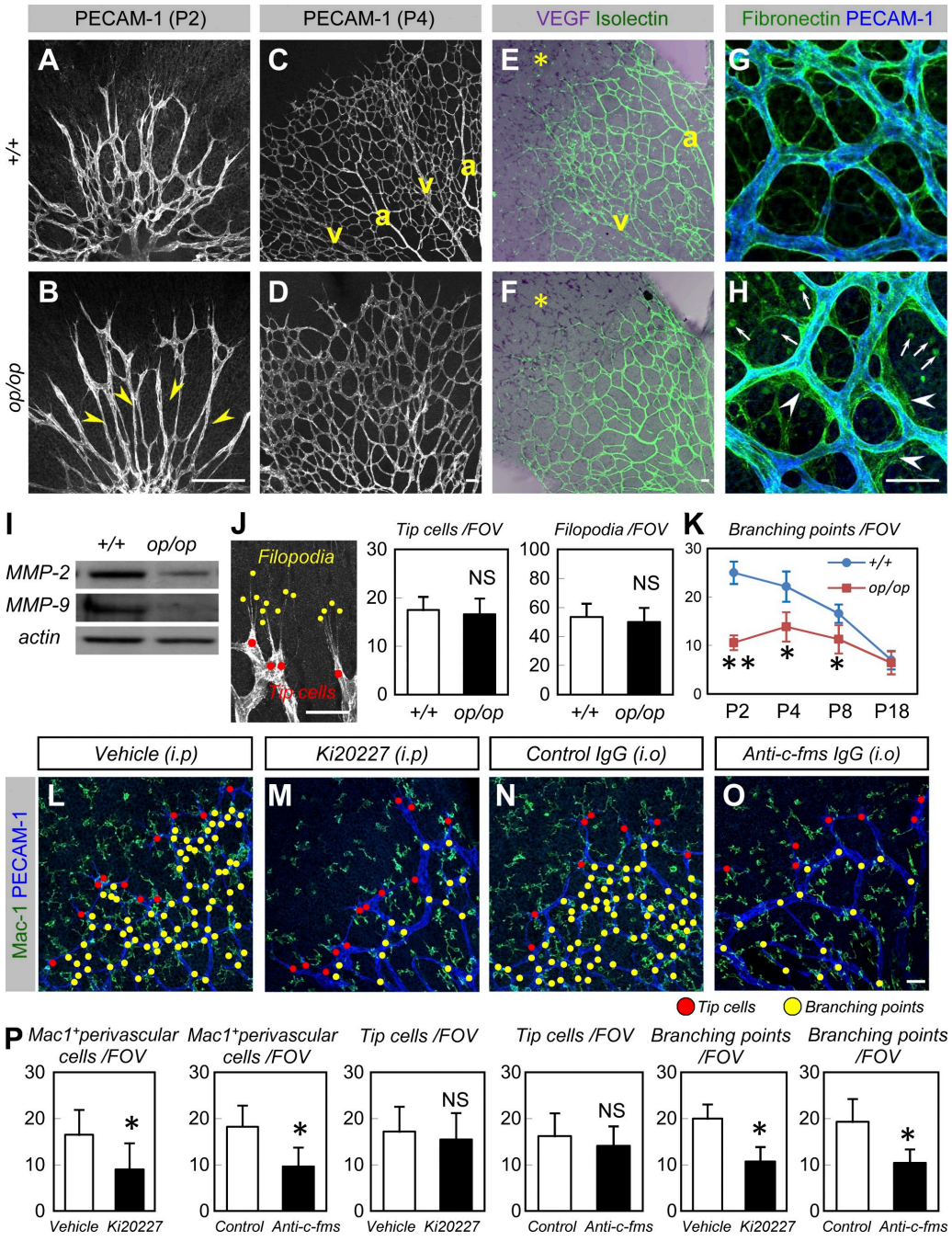

Figure 2. M-CSF contributes to developmental vascular remodeling. (A–D) An IHC analysis of PECAM-1 in P2 (A and B) and P4 (C and D) retinas (representative images of seven independent experiments). Note the reduced branching at P2 (indicated by arrowheads in B) and insufficient arterio-venous (a and v, respectively) patterning at P4 in *op/op* mice. (E and F) An ISH analysis of VEGF (purple) combined with isolectin B4 staining (green) at P4 (representative images of three independent experiments). VEGF expression (asterisks) was not altered in *op/op* mice. Also note the insufficient arterio-venous (a and v, respectively) patterning in *op/op* mice. (G and H) Double IHC of PECAM-1 (blue) and fibronectin (green) at P4 (representative images of four independent experiments). Note the irregular fibronectin proteins excessively deposited around the endothelial tubes (arrowheads) and rounded debris in the parenchymal area (arrows) in *op/op* mice. (I) Western blots of MMP-2 and MMP-9 in the P4 retina. Expression of MMP-2 and -9 decreased in the *op/op* mice. Representative panels are shown from three independent experiments. (J) The number of tip cells and filopodia (mean ± SD) were quantified as shown on the left ($n = 7$). (K) Quantification (mean ± SD) of branching points ($n = 7$). (L–O) Double IHC of Mac-1 (green) and PECAM-1 (blue) in P4 retinas after systemic treatment with vehicle (L) or Ki20227 (M) during P1–P4 or after intraocular injection with control IgG (N) or anti–c-fms IgG (O) at P1 (representative images of seven independent experiments). Note reduced branching points (yellow dots) and unaffected tip cells (red dots) in Ki20227-treated and anti–c-fms IgG-treated mice. Macrophages in retinas treated with Ki20227 and anti–c-fms antibodies exhibited insufficient stellate morphology and were present in lower numbers. (P) Quantification (mean ± SD) of Mac-1$^+$ perivascular cells, tip cells, or branching points ($n = 7$). Bars, 50 µm. *, $P < 0.05$; **, $P < 0.01$.

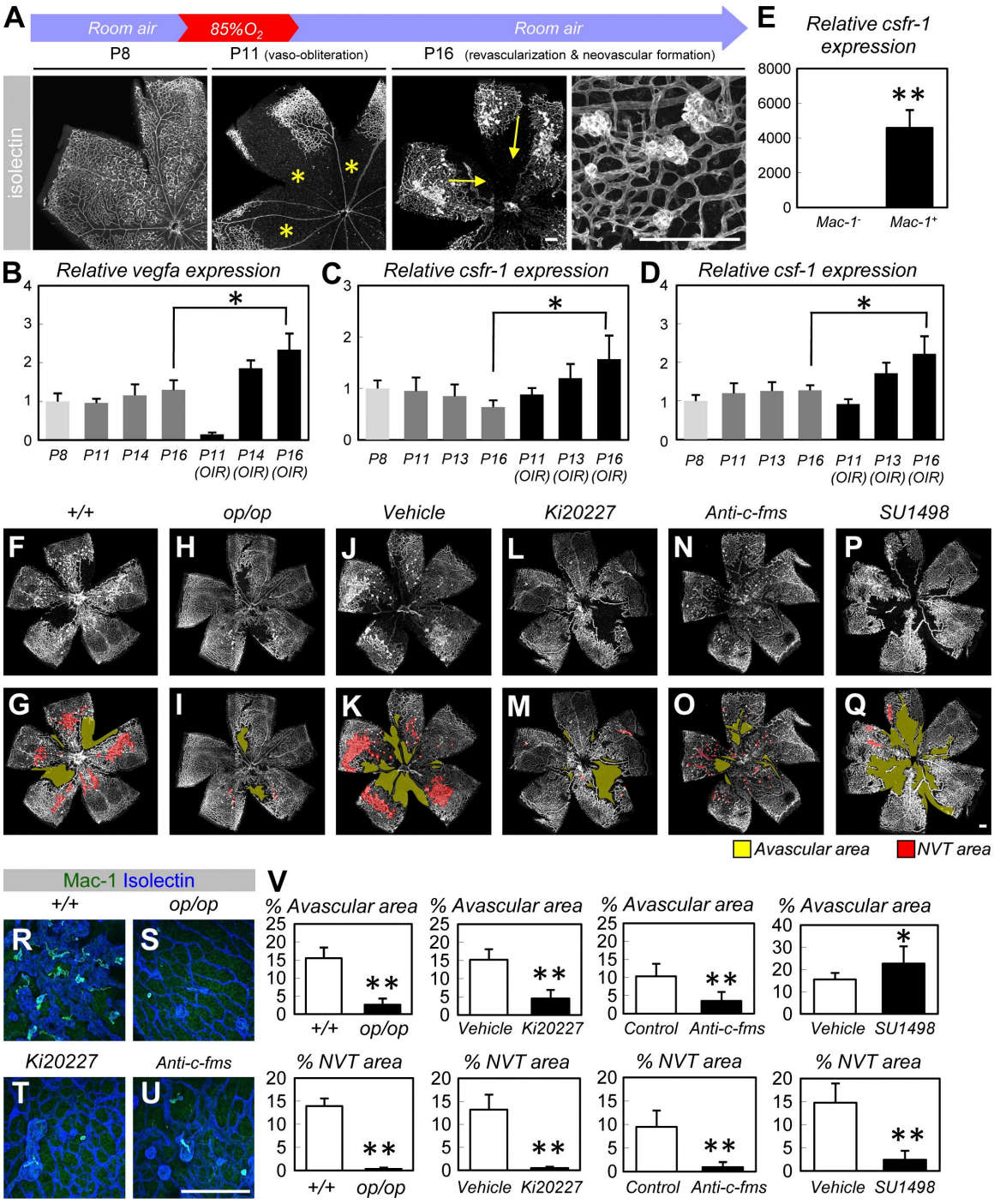

Figure 3. M-CSF is required for pathological neovascularization but not for the recovery of normal vasculature in OIR. (A) Isolectin staining of retinas in an OIR model. The central area of established vasculature was obliterated by hyperoxic insult, resulting in an avascular area (asterisks). After returning the mice to room air, normal vasculature was recovered via revascularization (arrows), although NVTs proliferated toward the vitreous body. (B–D) Relative expression (mean ± SD) of *vegf-a* (B), *csfr-1* (C), or *csf-1* (D) in retinal tissues exposed to normoxic conditions or in an OIR model ($n = 5$; all experiments were performed in quadruplicate and the mean for each sample was obtained). (E) Relative expression (mean ± SD) of *csfr-1* in FACS-sorted Mac-1$^+$ or Mac-1$^-$ cells obtained from P16 retinas in an OIR model ($n = 5$). (F–Q) Isolectin staining of P16 retinas in an OIR model (representative images of six independent experiments). Note the decreased avascular area (yellow) and NVT area (red) in *op/op* mice (H and I) and mice systemically treated with Ki20227 (L and M) during P12 and P16 or in mice that were given intraocular anti–c-fms antibodies during P12 (N and O). Systemic treatment with SU1498 decreased NVT area and increased avascular area (P and Q). (R–U) Double IHC of Mac-1 (green) and isolectin (blue) in the P16 retinas of an OIR model. Macrophages in *op/op* retinas or retinas treated with Ki20227/anti–c-fms antibodies were reduced in number and exhibited insufficient stellate morphology. (V) Quantification (mean ± SD) of the avascular area or NVT area ($n = 6$). Bars, 200 µm. *, $P < 0.05$; **, $P < 0.01$.

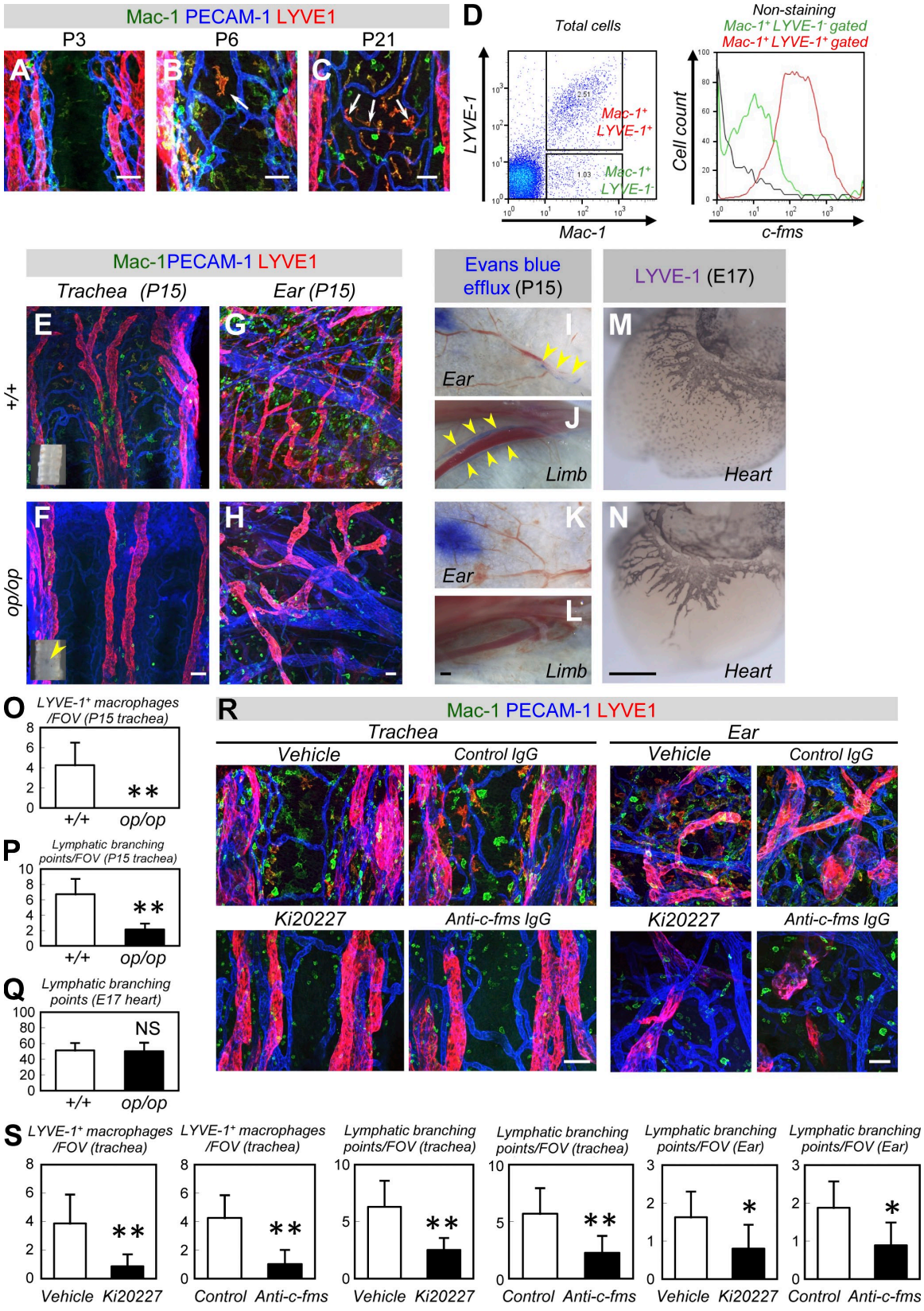

Figure 4. M-CSF contributes to postnatal lymphatic development. (A–C) Triple IHC of Mac-1 (green), LYVE-1 (red), and PECAM-1 (blue) in tracheas (representative images of four independent experiments). Note the LYVE-1+ macrophages in the vascularized area (arrows). (D) FACS analysis of dissociated

the number of LYVE1$^+$ macrophages correlate with the extent of tissue lymphangiogenesis (31). In the developing trachea, the emergence of LYVE-1$^-$ macrophages preceded that of LYVE-1$^+$ macrophages, and most LYVE-1$^+$ macrophages were present in vascularized areas (Fig. 4, A–C). Furthermore, c-fms expression was more abundant in LYVE-1$^+$ than in LYVE-1$^-$ macrophages (Fig. 4 D). As it is likely that M-CSF/c-fms signaling contributes to lymphangiogenesis, we examined developing lymphatic structures in *op/op* mice. At P15, the number of LYVE-1$^-$ and LYVE-1$^+$ macrophages dramatically decreased in the tracheas and ears of *op/op* mice, and reduced lymphatic branching was observed (Fig. 4, E–H, O, and P). Furthermore, tissue fluids drained more slowly in the limbs and ears of *op/op* mice (Fig. 4, I–L). By P15, some *op/op* mice exhibited apparent perforation of the dorsal tracheal surface (Fig. 4, E and F, insets), presumably as a result of abnormal lymphatic drainage. Although hydrocephalus is thought to underlie the high lethality of *op/op* mice at this stage (14), tracheal perforation could also lead to death. However, *op/op* mice that survived for 3 mo possessed normal lymphatic systems (unpublished data). The *op/op* mice exhibited normal embryonic lymphangiogenesis but lacked LYVE-1$^+$ macrophages (Fig. 4, M and N; and Fig. S3). Treatment with Ki20227 or anti–c-fms antibodies decreased both LYVE-1$^-$ and LYVE-1$^+$ macrophages and reduced the extent of lymphatic branching (Fig. 4, R and S). Collectively, these data show that M-CSF contributes to the appearance of LYVE-1$^+$ macrophages and postnatal lymphatic development.

M-CSF inhibition selectively suppresses tumor angiogenesis and lymphangiogenesis

The mechanisms underlying developmental angiogenesis and lymphangiogenesis may impact tumor angiogenesis and lymphangiogenesis (1, 2, 32); thus, we hypothesized that M-CSF–targeted therapies selectively suppress tumor angiogenesis and lymphangiogenesis. These effects may be especially noticeable in osteosarcomas, which express high levels of M-CSF (33). Therefore, we analyzed a mouse model of osteosarcoma, in which mice were transplanted with a newly established osteosarcoma cell line, AX (unpublished data). This line was established from c-Myc–overexpressing *Ink4a/ARF*$^{-/-}$ BM-derived stromal cells transfected with EGFP. Tumors grew actively in mice subcutaneously inoculated with AX cells and were accompanied by intratumor high-density vascularization and abundant peritumoral lymphatics (Fig. 5, A–E). To analyze the effects of M-CSF inhibition, Ki20227 or anti–c-fms antibodies were administered via daily subcutaneous injections. Mice treated with Ki20227 or anti–c-fms antibodies exhibited suppressed tumor growth, dramatically decreased tumor vascularization and peritumoral lymphatics (Fig. 5, A–G and Q–T), and decreased BrdU incorporation by tumor cells relative to control mice (Fig. 5, H–J, U, and V). Although small calcified loci were detected at the center of tumors in vehicle-treated mice, early and massive calcified loci were detected throughout the transplanted tumors in mice treated with Ki20227 or anti–c-fms antibodies (Fig. 5, K–M). Mice treated with Ki20227 or anti–c-fms antibodies exhibited dramatically decreased peritumoral LYVE-1$^+$ macrophages and perivascular macrophages infiltrated into tumors compared with control mice (Fig. 5, N–P). In contrast to VEGFR2 neutralization (11), continuous treatment of adult mice with Ki20227 or anti–c-fms antibodies for a period of 56 d did not affect healthy vascular and lymphatic systems outside the tumor (Fig. 5 W). Collectively, M-CSF inhibition selectively suppressed tumor angiogenesis and lymphangiogenesis.

We performed in vitro culture experiments to determine if the tumor-suppressing effects of c-fms inhibition are mediated by effects on tumors or on recruited monocytes. Hypoxic growth resulted in osteogenic differentiation and M-CSF expression and decreased proliferation in cultured AX cells (Fig. S4, A–C). However, supplementation with 100 nM Ki20227, a sufficient dose for the inhibition of c-fms kinase (27), did not affect osteogenic differentiation or proliferation in AX cells (Fig. S4, A and F). Supplementation with 100 nM Ki20227 inhibited survival and proliferation in cultured BM mononuclear cells (MNCs; unpublished data). To identify the potential ligand–receptor interactions resulting from M-CSF signaling between tumors and macrophages, we compared the expression of M-CSF and c-fms in cultured AX cells and in BM MNCs. Cultured AX cells exhibited high levels of *csf-1* expression, compared with cultured MNCs (Fig. S4 D), but relatively lower levels of *csfr-1* (Fig. S4 E) expression. These in vitro data suggest that the tumor-suppressing effects of M-CSF inhibition are mediated by effects on recruited macrophages but do not directly affect AX cells.

cells (a representative plot of three independent experiments). Note the more abundant expression of c-fms in LYVE-1$^+$ than in LYVE-1$^-$ macrophages. (E–H) Whole-mount IHC of Mac-1 (green), LYVE-1 (red), and PECAM-1 (blue) in P15 tracheas (E and F) or ears (G and H; representative images of six independent experiments). Note the reduced lymphatic branching in *op/op* mice. Insets in E and F indicate bright field views of P15 trachea. Note the perforation typically seen in *op/op* mice (arrowhead). (I–L) Lymphangiography in ears (I and K) and limbs (J and L; representative images of three independent experiments). Note that the blue dye (arrowheads) observed in the lymphatic ducts of wild-type mice is not seen in *op/op* mice. (M and N) Whole-mount IHC of LYVE-1 in the hearts of E17 embryos (representative images of three independent experiments). The *op/op* mice exhibited normal lymphangiogenesis, although they lacked LYVE-1$^+$ macrophages. (O–Q) Quantification (mean ± SD) of LYVE-1$^+$ macrophages or lymphatic branching points (n = 6 [O and P]; n = 3 [Q]). (R) Triple IHC of Mac-1 (green), LYVE-1 (red), and PECAM-1 (blue) in P15 tracheas or ears systemically treated with vehicle (methylcellulose), Ki20227, control IgG, or anti–c-fms IgG during P8 and P15. Treatment with Ki20227 or anti–c-fms IgG decreased LYVE-1$^-$ and LYVE-1$^+$ macrophages and reduced lymphatic branching (representative images of six independent experiments). (S) Quantification (mean ± SD) of LYVE-1$^+$ macrophages or lymphatic branching points (n = 6). Bars: (I–N) 200 µm; (A–C, E–H, and R) 50 µm. *, $P < 0.05$; **, $P < 0.01$.

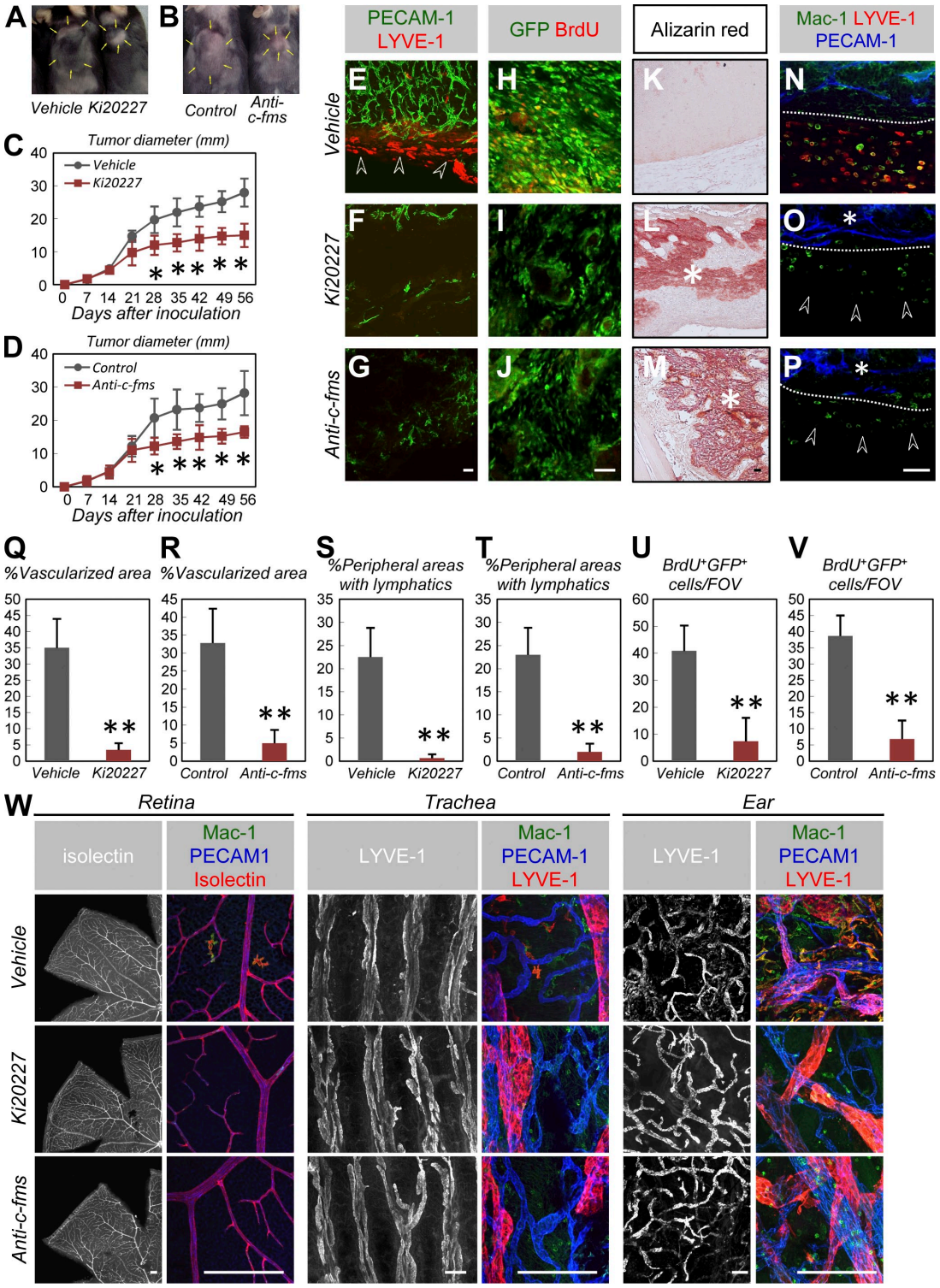

Figure 5. M-CSF inhibition selectively suppresses tumor angiogenesis and lymphangiogenesis in mouse osteosarcoma. (A and B) Typical appearance of mice 42 d after transplantation with AX cells. Arrows indicate tumor areas. (C and D) Quantification (mean ± SD) of tumor diameter (n = 5). (E–G) An IHC analysis of PECAM-1 (green) and LYVE-1 (red) in tumors 21 d after transplantation (representative images of seven independent experiments). Arrowheads in E indicate peritumoral lymphatics. Treatment with Ki20227 or anti–c-fms IgG decreased the amount of associated vascularization and peritumoral lymphatics. (H–M) An IHC analysis using GFP (green) and BrdU (red; H–J) or Alizarin red staining (K–M; representative images of five independent experiments). Treatment with Ki20227 or anti–c-fms IgG decreased BrdU incorporation into tumor cells but increased tumor calcification (asterisks). (N–P) An IHC analysis of Mac-1 (green), PECAM-1 (blue), and LYVE-1 (red) in tumors 21 d after transplantation. Dotted lines indicate tumor

M-CSF inhibition suppresses tumor metastasis of mouse osteosarcoma and improves prognosis

We then examined the effects of Ki20227 and anti–c-fms antibodies on tumor metastasis and disease prognosis. We performed a functional analysis of tumor-associated lymphatics by examining the dye efflux capacity of transplanted tumors. Tumors in mice treated with Ki20227 or anti–c-fms antibodies exhibited significantly higher levels of dye retention compared with tumors in vehicle-treated mice (Fig. 6, A–C and V). In vehicle-treated mice, transplanted AX cells spread to the liver and lung (Fig. 6, D, G, J, M, P, and S), two major metastatic sites in human osteosarcoma (20). Approximately 20% of mice remained alive 56 d after tumor cell inoculation (Fig. 6 X). However, metastases were dramatically suppressed in mice treated with Ki20227 or anti–c-fms antibodies (Fig. 6, D–U and W), and >90% of these mice survived for 56 d (Fig. 6 X). Aside from its role in M-CSF/c-fms signaling, VEGF/Flt1 plays a profound role in the recruitment of macrophages and the progression of cancer in various models (11, 34–36). To examine the involvement of VEGF/Flt1 signaling in our established mouse osteosarcoma, AX cells were transplanted into mice deficient in Flt1 tyrosine kinase (*Vegfr1 tk*$^{-/-}$). Deficiency in Flt1 tyrosine kinase did not affect the number of recruited macrophages (Fig. S5, A and B), tumor growth (Fig. S5 C), or metastasis (Fig. S5, D–G), suggesting that macrophages are less dependent on VEGF/Flt1 signaling in this model than in other cancer models.

M-CSF inhibition disorganizes extracellular matrices and suppresses tumor progression when treatment is interrupted

To explore the differences between M-CSF inhibition and VEGF inhibition, we compared the antitumor effects of two small tyrosine kinase inhibitors, Ki20227 and SU1498. Vascular ECM structures stained by fibronectin (which has the potential to induce tumor vascular regrowth) (8) retained the spatial distribution surrounding endothelial cells treated with SU1498 or a vehicle (Fig. 7, A–F). In contrast, these structures were irregularly deposited throughout the tumors in Ki20227-treated mice (Fig. 7, G–L), suggesting a disturbance in the remodeling or degradation of ECM scaffolds. In contrast to Ki20227, SU1498 did not affect tumor-associated macrophages (Fig. 7, M and N). Tumors transplanted into MMP-9$^{-/-}$ mice exhibited irregularly deposited ECM structures, which is similar to tumors transplanted into Ki20227-treated mice (Fig. 7, O and P), and exhibited decreased tumor growth (not depicted). These data suggest that the proteases produced by macrophages contribute to matrix remodeling. Furthermore, we compared the antitumor effects of M-CSF inhibition and VEGF inhibition in three differential therapeutic protocols, including the protocol that involved interruption of administration in addition to vehicle or continuous treatment (Fig. 7 Q). Although continuous SU1498 administration greatly inhibited tumor growth and vascular/lymphatic growth in tumors, as did Ki20227 administration, interruption of SU1498 treatment resulted in rapid vascular and lymphatic regrowth (Fig. 7, S–U). In contrast, interruption of Ki20227 administration greatly reduced vascular and lymphatic growth (Fig. 7, V–X). Although the interruption of SU1498 treatment did not sufficiently inhibit tumor metastasis and cancer death, sustained effectiveness was observed after the interruption of Ki20227 administration (Fig. 7, Y, Z, and AA).

DISCUSSION

We used *op/op* mice to demonstrate that M-CSF–dependent macrophages contribute to both vascular and lymphatic development. Furthermore, we show that M-CSF is required for pathological neovascularization but not for the recovery of normal vasculature in OIR. Deficiency in M-CSF does not affect the maintenance of stable adult vasculature and lymphatics. In mice with osteosarcoma, M-CSF inhibition selectively suppressed tumor angiogenesis and lymphangiogenesis and decreased tumor regrowth after the interruption of treatment.

Our data showing the highly specific effects of M-CSF inhibition on pathological angiogenesis and lymphangiogenesis are supported by the observation that no detectable abnormalities in adult vascular and lymphatic systems were found in *op/op* mice. In contrast to the effects of VEGF blockade, interruption of M-CSF inhibition did not promote rapid tumor regrowth but rather improved the prognosis relative to treatment with a vehicle. This difference might be a result of the effects of M-CSF inhibition on the "sleeves" of the basement membrane. These so-called sleeves are conserved during VEGF blockade and assist with rapid vascular regrowth in primary tumors (8). The physiological role of retinal macrophages in developmental vascular remodeling, but not in angiogenic sprouting, suggests that M-CSF inhibition and VEGF blockade target different factors. Indeed, the tumor-suppressive effects of M-CSF inhibition are independent of VEGF signaling. Furthermore, a recent study showed that tumor refractoriness to anti-VEGF treatment is mediated by Mac-1^{+}Gr1^{+} myeloid cells (37), suggesting that M-CSF–targeted therapy may serve as a useful secondary therapy in patients who are resistant to VEGF blockade.

We showed that retinal macrophages express high levels of MMP-2 and MMP-9 but not VEGF. These expression patterns

margins. Treatment with Ki20227 or anti–c-fms IgG decreased the peritumoral LYVE-1^{+} macrophages (arrowheads) and perivascular macrophages (asterisks) into tumors (representative images of seven independent experiments). (Q–T) Quantification (mean ± SD) of vascularized areas (Q and R) or peripheral areas with lymphatics (S and T; $n = 7$). (U and V) Quantification (mean ± SD) of BrdU^{+}GFP^{+} cells ($n = 5$). (W) An IHC analysis using the indicated antibodies for adult retina, trachea, or ears after 56 d of treatment (representative images of four independent experiments). No vascular and lymphatic abnormalities were observed in mice treated with Ki20227 or anti–c-fms IgG, although these treatments decreased LYVE-1^{-} and LYVE-1^{+} macrophages. Bars: (W) 200 µm; (E–P) 50 µm. *, $P < 0.05$; **, $P < 0.01$.

are thought to reflect the vascular defects in *op/op* mice, which are characterized by normal sprouting angiogenesis and impaired vascular remodeling. Although VEGF plays a critical role in angiogenic sprouting (26), MMP-2 and MMP-9 are gelatinase proteinases with overlapping substrates (e.g., fibronectin) that function together in some situations such as aortic aneurysms (24). One of the major questions in our study is whether disordered fibronectin architecture, which is presumably caused by the absence of macrophage MMP-2 and MMP-9, is the primary cause of vascular defects in *op/op* mice. However, the precise function of specific proteinases is generally difficult to discern because of the considerable redundancy of these enzymes (24). In fact, MMP-9$^{-/-}$ mice exhibit normal vascular development and normal ECM structures in their developing retina (unpublished data), which is in contrast to the dramatically decreased NVTs observed in the OIR model. Clinical observations of diabetic microvessels in humans have revealed that disordered fibronectin structures are the earliest events preceding various capillary defects (38). These observations also support the idea that disordered fibronectin architecture accounts for defects associated with impaired vascular remodeling in the *op/op* retina.

Previous studies have shown that M-CSF/c-fms signaling promotes the differentiation of circulating monocytes into

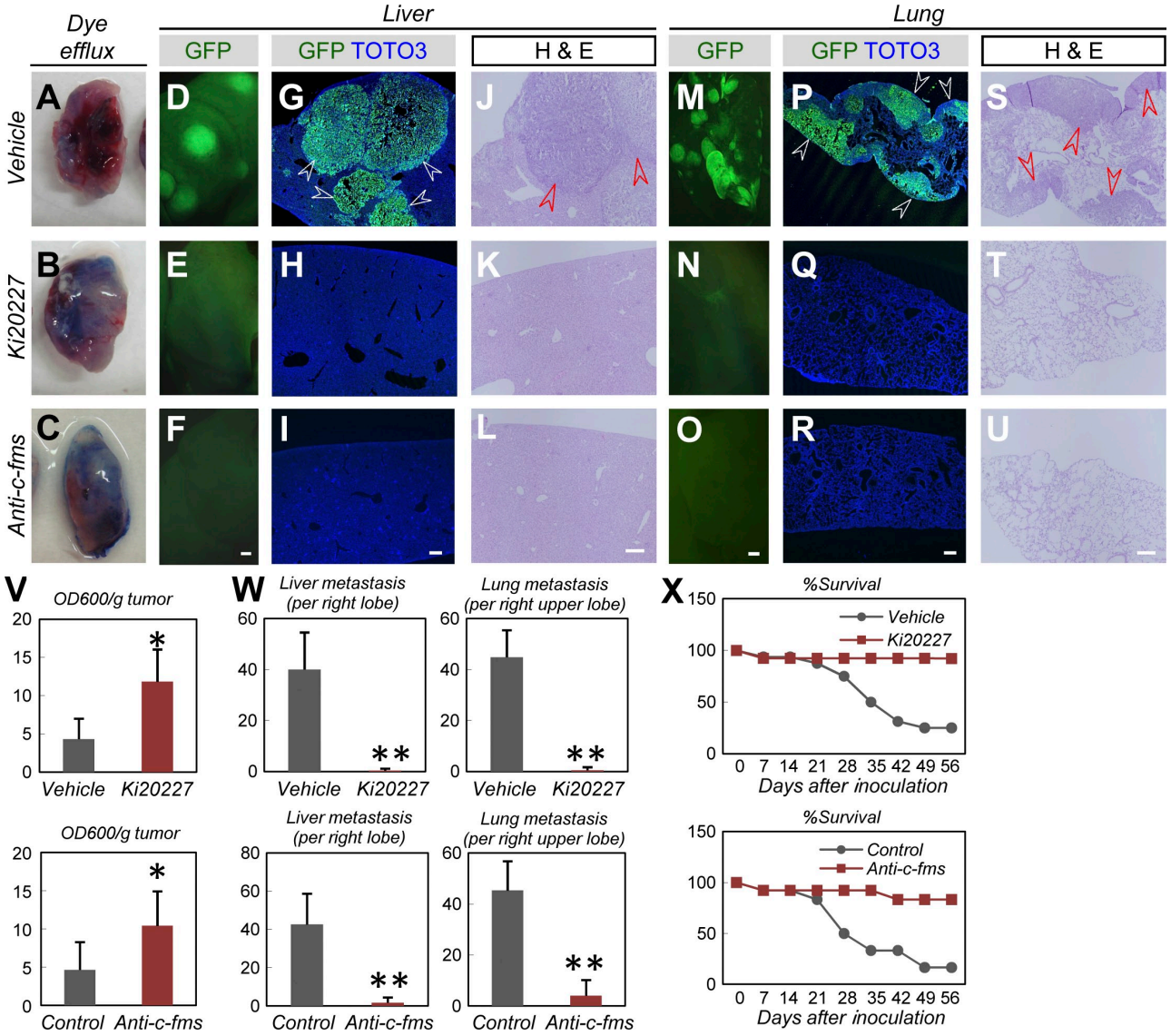

Figure 6. M-CSF inhibition suppresses tumor metastasis of mouse osteosarcoma and improves prognosis. (A–C) Representative appearance of tumors 2 h after injection with Evans blue dye (representative images of five independent experiments). (D–U) Fluorescent views (D–F and M–O), IHC for GFP (green) and TOTO3 (blue; G–I and P–R), or hematoxylin and eosin staining (J–L and S–U) in the liver or lung 56 d after tumor inoculation (representative images of five independent experiments). Note that the multiple metastatic masses (arrowheads) in control mice were completely absent in mice treated with Ki20227/anti-c-fms IgG. (V–X) Quantification (mean ± SD) of the OD600 measurements of extracted dye (V; $n = 5$), liver and lung metastasis at day 56 (W; $n = 5$), and survival rate (X; at least six mice were examined in each group). Bars, 200 µm. *, $P < 0.05$; **, $P < 0.01$.

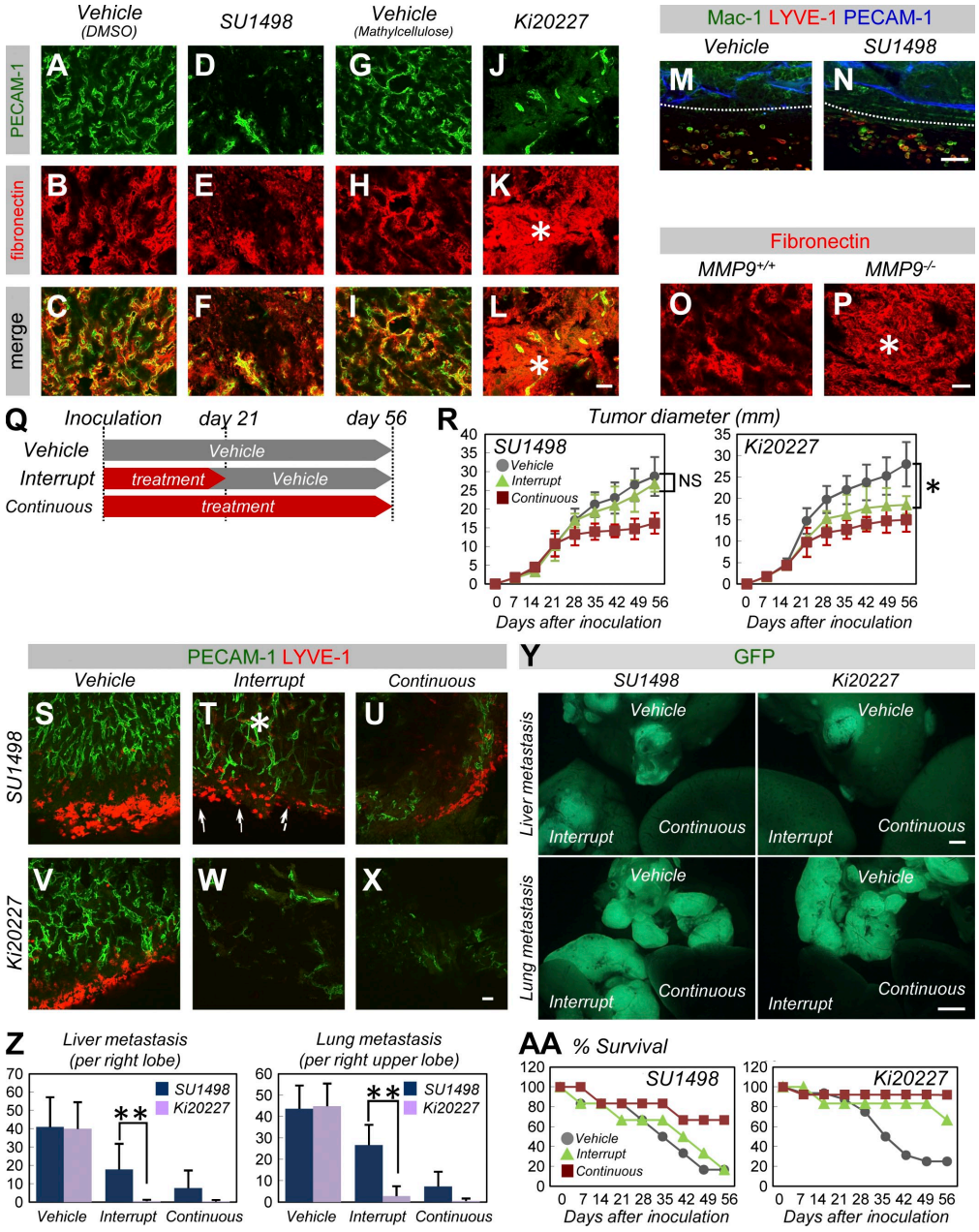

Figure 7. M-CSF inhibition disorganizes extracellular matrices and suppresses tumor progression when treatment is interrupted. (A–L) An IHC analysis of PECAM-1 (green) and fibronectin (red) in tumors 21 d after transplantation (representative images of three independent experiments). Note that massively deposited fibronectin proteins were distributed throughout the tumors (asterisks) in Ki20227-treated mice but not in SU1498-treated mice, whereas tumor vasculature decreased in both mice. (M and N) An IHC analysis of Mac-1 (green), PECAM-1 (blue), and LYVE-1 (red) in tumors 21 d after transplantation (representative images of three independent experiments). Dotted lines indicate tumor margins. Treatment with SU1498 did not affect LYVE-1$^-$ or LYVE-1$^+$ macrophages. (O and P) Fibronectin staining of tumors 21 d after transplantation into *MMP-9*$^{+/+}$ or *MMP-9*$^{-/-}$ mice (representative images of three independent experiments). Note the presence of massively deposited fibronectin proteins (asterisk) in the *MMP-9*$^{-/-}$ mice. (Q) A modified scheme involving the administration of small molecule inhibitors. Administration was either continuous for 56 d (continuous) or terminated at day 21 (interrupt) after tumor inoculation. (R) Quantification (mean ± SD) of tumor diameter (more than five mice were examined in each regimen). (S–X) An IHC analysis of PECAM-1 (green) and LYVE-1 (red) in tumors 21 d after transplantation (representative images of three independent experiments). Although continuous SU1498 administration greatly inhibited vascular and lymphatic growth, interruption of treatment resulted in rapid vascular (asterisk) and lymphatic (arrows) regrowth. In contrast, Ki20227 reduced vasculature and lymphatics even after the interruption of treatment. (Y) Fluorescent views of liver or lung at day 56 in each regimen (representative images of five independent experiments). Although the interruption of SU1498 treatment caused multiple tumor metastases (as in vehicle treatment), metastatic masses were greatly reduced when Ki20227 treatment was interrupted. (Z) Quantification (mean ± SD) of liver and lung metastases at day 56 in each regimen ($n = 5$). (AA) Survival rate (more than five mice were examined in each regimen). Bars: (Y) 1 mm; (A–P and S–X) 50 µm. *, $P < 0.05$; **, $P < 0.01$.

macrophages (13). However, abundant c-fms expression by LYVE-1$^+$ macrophages and defective postnatal lymphangiogenesis in *op/op* mice suggests that M-CSF also acts on LYVE-1$^+$ macrophages and lymphangiogenesis. The link between the absence of LYVE1$^+$ cells and reduced lymphangiogenesis may be explained by reductions in the secretion of VEGF-C, VEGF–D, or other inflammatory cytokines by LYVE1$^+$ macrophages (11, 31, 32). The significant contribution of BM-derived lymphatic endothelial progenitor cells to lymphangiogenesis (39) may be responsible for this link.

Other than M-CSF/c-fms signaling, VEGF/Flt1 signaling significantly contributes to the recruitment of macrophages and tumor progression in various cancer models (11, 34–36). In our osteosarcoma model (in which tumor cells expressed high levels of M-CSF, just as in human osteosarcoma), deficiency in Flt1 tyrosine kinase did not significantly affect tumor progression. These data suggest that tumor progression depends primarily on M-CSF/c-fms signaling rather than on VEGF/Flt1 signaling. In addition, the *Vegfr1 tk*$^{-/-}$ mice in the OIR model did not experience a significant reduction in the amount of NVT or in the number of recruited macrophages (unpublished data). However, decreases in the number of tumor-associated macrophages observed in *Vegfr1 tk*$^{-/-}$ mice in other cancer models suggest that VEGF/Flt1 signaling plays an important role in the recruitment of macrophages and that Flt1-targeted therapy also holds potential as a tumor-selective strategy. It would be interesting to determine the extent to which M-CSF/c-fms or VEGF/Flt1 signaling affects macrophage recruitment in various other cancer models.

Overall, our data show that M-CSF inhibition efficiently suppresses pathological angiogenesis and lymphangiogenesis in mice with ischemic retinopathy and osteosarcoma. This highly selective chemotherapy, which does not affect healthy tissues or induce toxic side effects, may be an ideal treatment for ocular neovascular diseases and cancer.

MATERIALS AND METHODS

Mice and hyperoxia exposure. The C57BL/6 mice (Japan SLC, Inc.), *op/op* mice (The Jackson Laboratory), MMP-9$^{-/-}$ mice (The Jackson Laboratory), and *Vegfr1 tk*$^{-/-}$ mice (34, 35) were used. All animal experiments were approved by Keio University and were performed in accordance with the Guidelines of Keio University for Animal and Recombinant DNA experiments. The P8 mice and nursing mothers used in the OIR model were maintained for 3 d in 85% oxygen and then placed in room air (40). To examine c-fms inhibition, mice were subcutaneously injected once daily from P8 to P11 or from P11 to P16 with 50 mg/kg (body weight [BW]) of Ki20227 (27) dissolved in 100 µl methylcellulose or vehicle.

Preparation of whole-mount samples. Isolated eyes, tracheas, and other tissues were fixed for 20 min in 4% paraformaldehyde (PFA) in PBS and dissected as previously described (31, 40). Tissues were postfixed and stored in methanol at −20°C. The tissue samples were gradually rehydrated for further analysis.

Whole-mount IHC and ISH. IHC analysis of whole-mount samples was performed as previously described (31, 40). For whole-mount retinal ISH, retinas were briefly digested with proteinase K and hybridized with digoxigenin-labeled antisense RNA probes.

Antibodies for IHC. Primary monoclonal antibodies used include hamster anti–PECAM-1 (2H8; Millipore), rat anti–PECAM-1 (MEC13.3; BD), Mac-1 (M1/7; BD), F4/80 (A3-1; AbD Serotec), PDGFR-α (APA5; eBioscience), and desmin (Dako). Primary polyclonal antibodies included Alexa Fluor 488–conjugated anti-GFP (Invitrogen), MMP-9 (Santa Cruz Biotechnology, Inc.), collagen IV (Cosmo Bio), LYVE-1 (ReliaTech), and fibronectin (Dako). Secondary antibodies included Alexa Fluor 488 fluorescence-conjugated IgGs (Invitrogen) or Cy3/Cy5-conjugated IgGs (Jackson ImmunoResearch Laboratories). In preparation for nuclear staining, specimens were treated with TOTO3 (Invitrogen) or DAPI (Invitrogen). In some experiments, blood vessels and monocyte lineage cells were simultaneously visualized using biotinylated isolectin B4 (Sigma-Aldrich), followed by treatment with fluorescent streptavidin conjugates (Invitrogen).

Tumor inoculation and c-fms inhibitor treatment. The AX cells were cultured in DMEM containing 10% FCS, and the medium was changed daily. Approximately 2×10^6 cells in subconfluent culture were resuspended in 200 µl of medium and were subcutaneously transplanted into the back of mice. The following was injected daily into subcutaneous tissues at the base of the tail: ∼50 mg/kg (BW) of Ki20227 (27) dissolved in 200 µl methylcellulose; 50 mg/kg (BW) of AFS98, a rat monoclonal anti-murine c-fms antibody (IgG2a; provided by S.-I. Nishikawa and S. Nishikawa, Riken Center for Developmental Biology, Kobe, Japan) (28), dissolved in 200 µl of PBS; an isotype-matched irrelevant rat IgG dissolved in 200 µl of PBS; 9 mg/kg (BW) of SU1498 (EMD) dissolved in 100 µl of DMSO; or vehicle only. Metastatic lesions were enumerated by counting detectable GFP$^+$ masses under a fluorescent microscope.

Intraocular injections. Injections into the vitreous body were performed using 33-gauge needles, as described previously (26, 40). Approximately 1 mg/ml AFS98 or an isotype-matched irrelevant rat IgG dissolved in ∼50 nl of sterile PBS was injected on P1 or P12 (OIR).

Lymphangiography. Functional lymphatic vessels were visualized by injecting 20 µl of Evans blue dye (5 mg/ml; Sigma-Aldrich) into the hindlimb footpad or the ear, and lymphatic vessels were analyzed via light microscopy. In preparation for the tumor dye efflux experiment, we injected 50 µl of Evans blue dye into tumors and sacrificed animals 2 h later. Approximately 100 mg of tumors were dissected and incubated in 1 ml formamide (to extract the Evans blue dye), and the absorbency was measured at OD600 using a spectrophotometer.

Quantitative RT-PCR analysis. Total RNA was prepared from cultured cells and reverse transcribed using Superscript II (Invitrogen). Quantitative PCR was performed on an ABI 7500 Fast Real-Time PCR system using the TaqMan Fast Universal PCR master mix (Applied Biosystems) and a TaqMan Gene Expression Assay mixture containing *csf-1* (Mm00432688_m1), *csfr-1* (Mm00432689_m1), or *vegf-a* (Mm00437304_m1). A mouse β-actin (Mm00607939_s1) mixture served as an endogenous control. Data were analyzed using 7500 Fast System SDS Software 1.3.1. All experiments were performed in quadruplicate and a mean was obtained for each sample.

FACS analysis. Dissected tracheas were incubated at 37°C for 30 min in DMEM containing 1% collagenase D (from *Clostridium histolyticum*; Roche) before dissociation by gentle trituration. Harvested cells were immunostained, followed by purification and analysis using the FACSVantage (BD).

Confocal microscopy. Fluorescence images were obtained using a confocal laser-scanning microscope (FV1000; Olympus). Scanning was performed in sequential laser emission mode to avoid scanning at other wavelengths. Cells or substances of interest were quantified in eight (200 µm × 200 µm) fields of view per sample in each scanned image, and the mean of eight fields was determined.

Statistical analysis. Results were expressed as means ± SD. The means of two groups were compared using a two-tailed Student's *t* test. P-values <0.05 were considered statistically significant.

Online supplemental material. Fig. S1 shows normal vascular structure in *op/op* mice at P8 and P90. Fig. S2 shows that M-CSF deficiency or M-CSF

inhibition does not affect vaso-obliteration in OIR model. Fig. S3 shows that various embryonic tissues in *op/op* mice exhibit normal lymphangiogenesis but lacked LYVE-1$^+$ macrophages. Fig. S4 shows that hypoxia, but not Ki20227, induces osteogenic differentiation and decreases proliferation in cultured AX cells. Fig. S5 shows that there is no significant difference between *Vegfr1 tk*$^{+/+}$ and *Vegfr1 tk*$^{-/-}$ in tumor progression when transplanted with AX cells. Online supplemental material is available at http://www.jem.org/cgi/content/full/jem.20081605/DC1.

We would like to thank Holger Gerhardt (Vascular Biology Laboratory, London Research Institute, UK), Donald M. McDonald (Cardiovascular Research Institute, University of California, San Francisco), and Takeshi Miyamoto (Keio University) for their helpful discussions and critical review of our manuscript. AFS98 was kindly provided by Shin-Ichi Nishikawa and Satomi Nishikawa (Riken Center for Developmental Biology, Kobe, Japan).

This work was supported by Grants-in-Aid for Specially Promoted Research from the Ministry of Education, Culture, Sports, Science and Technology of Japan, by a grant from the Mitsubishi Pharma Research Foundation, by a grant from the Tokyo Biochemical Research Foundation, and by the Keio Kanrinmaru Project.

The authors have no conflicting financial interests.

Submitted: 22 July 2008
Accepted: 3 April 2009

REFERENCES

1. Carmeliet, P. 2005. Angiogenesis in life, disease and medicine. *Nature*. 438:932–936.
2. Ferrara, N., and R.S. Kerbel. 2005. Angiogenesis as a therapeutic target. *Nature*. 438:967–974.
3. Rudge, J.S., G. Thurston, S. Davis, N. Papadopoulos, N. Gale, S.J. Wiegand, and G.D. Yancopoulos. 2005. VEGF trap as a novel antiangiogenic treatment currently in clinical trials for cancer and eye diseases, and VelociGene-based discovery of the next generation of angiogenesis targets. *Cold Spring Harb. Symp. Quant. Biol.* 70:411–418.
4. Holash, J., S. Davis, N. Papadopoulos, S.D. Croll, L. Ho, M. Russell, P. Boland, R. Leidich, D. Hylton, E. Burova, et al. 2002. VEGF-Trap: a VEGF blocker with potent antitumor effects. *Proc. Natl. Acad. Sci. USA*. 99:11393–11398.
5. Pieramici, D.J., and M.D. Rabena. 2008. Anti-VEGF therapy: comparison of current and future agents. *Eye*. 22:1330–1336.
6. Maharaj, A.S., T.E. Walshe, M. Saint-Geniez, S. Venkatesha, A.E. Maldonado, N.C. Himes, K.S. Matharu, S.A. Karumanchi, and P.A. D'Amore. 2008. VEGF and TGF-β are required for the maintenance of the choroid plexus and ependyma. *J. Exp. Med.* 205:491–501.
7. Verheul, H.M., and H.M. Pinedo. 2007. Possible molecular mechanisms involved in the toxicity of angiogenesis inhibition. *Nat. Rev. Cancer*. 7:475–485.
8. Mancuso, M.R., R. Davis, S.M. Norberg, S. O'Brien, B. Sennino, T. Nakahara, V.J. Yao, T. Inai, P. Brooks, B. Freimark, et al. 2006. Rapid vascular regrowth in tumors after reversal of VEGF inhibition. *J. Clin. Invest.* 116:2610–2621.
9. Saharinen, P., and K. Alitalo. 2003. Double target for tumor mass destruction. *J. Clin. Invest.* 111:1277–1280.
10. Shojaei, F., X. Wu, C. Zhong, L. Yu, X.H. Liang, J. Yao, D. Blanchard, C. Bais, F.V. Peale, N. van Bruggen, et al. 2007. Bv8 regulates myeloid-cell-dependent tumour angiogenesis. *Nature*. 450: 825–831.
11. Fischer, C., B. Jonckx, M. Mazzone, S. Zacchigna, S. Loges, L. Pattarini, E. Chorianopoulos, L. Liesenborghs, M. Koch, M. De Mol, et al. 2007. Anti-PlGF inhibits growth of VEGF(R)-inhibitor-resistant tumors without affecting healthy vessels. *Cell*. 131:463–475.
12. Sherr, C.J., C.W. Rettenmier, R. Sacca, M.F. Roussel, A.T. Look, and E.R. Stanley. 1985. The c-fms proto-oncogene product is related to the receptor for the mononuclear phagocyte growth factor, CSF-1. *Cell*. 41:665–676.
13. Cecchini, M.G., M.G. Dominguez, S. Mocci, A. Wetterwald, R. Felix, H. Fleisch, O. Chisholm, W. Hofstetter, J.W. Pollard, and E.R. Stanley. 1994. Role of colony stimulating factor-1 in the establishment and regulation of tissue macrophages during postnatal development of the mouse. *Development*. 120:1357–1372.
14. Marks, S.C. Jr., and P.W. Lane. 1976. Osteopetrosis, a new recessive skeletal mutation on chromosome 12 of the mouse. *J. Hered*. 67: 11–18.
15. Lin, E.Y., J.F. Li, L. Gnatovskiy, Y. Deng, L. Zhu, D.A. Grzesik, H. Qian, X.N. Xue, and J.W. Pollard. 2006. Macrophages regulate the angiogenic switch in a mouse model of breast cancer. *Cancer Res*. 66:11238–11246.
16. Lin, E.Y., A.V. Nguyen, R.G. Russell, and J.W. Pollard. 2001. Colony-stimulating factor 1 promotes progression of mammary tumors to malignancy. *J. Exp. Med*. 193:727–740.
17. Aharinejad, S., P. Paulus, M. Sioud, M. Hofmann, K. Zins, R. Schäfer, E.R. Stanley, and D. Abraham. Colony-stimulating factor-1 blockade by antisense oligonucleotides and small interfering RNAs suppresses growth of human mammary tumor xenografts in mice. 2004. *Cancer Res*. 64: 5378–84.
18. Paulus, P., E.R. Stanley, R. Schäfer, D. Abraham, and S. Aharinejad. Colony-stimulating factor-1 antibody reverses chemoresistance in human MCF-7 breast cancer xenografts. 2006. *Cancer Res*. 66: 4349–56.
19. Zeisberger, S.M., B. Odermatt, C. Marty, A.H. Zehnder-Fjällman, K. Ballmer-Hofer, and R.A. Schwendener. Clodronate-liposome-mediated depletion of tumour-associated macrophages: a new and highly effective antiangiogenic therapy approach. 2006. Br. J. Cancer. 95: 272–81.
20. Renard, A.J., R.P. Veth, H.W. Schreuder, M. Pruszczynski, J.P. Bokkerink, Q.G. van Hoesel, and F.J. van Der Staak. 1999. Osteosarcoma: Oncologic and functional results. A single institutional report covering 22 years. *J. Surg. Oncol*. 72:124–129.
21. Gariano, R.F., and T.W. Gardner. 2005. Retinal angiogenesis in development and disease. *Nature*. 438:960–966.
22. Ridgway, J., G. Zhang, Y. Wu, S. Stawicki, W.C. Liang, Y. Chanthery, J. Kowalski, R.J. Watts, C. Callahan, I. Kasman, et al. 2006. Inhibition of Dll4 signalling inhibits tumour growth by deregulating angiogenesis. *Nature*. 444:1083–1087.
23. Fruttiger, M. 2007. Development of the retinal vasculature. *Angiogenesis*. 10:77–88.
24. Sternlicht, M.D., and Z. Werb. 2001. How matrix metalloproteinases regulate cell behavior. *Annu. Rev. Cell Dev. Biol*. 17:463–516.
25. Lobov, I.B., S. Rao, T.J. Carroll, J.E. Vallance, M. Ito, J.K. Ondr, S. Kurup, D.A. Glass, M.S. Patel, W. Shu, et al. 2005. WNT7b mediates macrophage-induced programmed cell death in patterning of the vasculature. *Nature*. 437:417–421.
26. Gerhardt, H., M. Golding, M. Fruttiger, C. Ruhrberg, A. Lundkvist, A. Abramsson, M. Jeltsch, C. Mitchell, K. Alitalo, D. Shima, and C. Betsholtz. 2003. VEGF guides angiogenic sprouting utilizing endothelial tip cell filopodia. *J. Cell Biol*. 161:1163–1177.
27. Ohno, H., K. Kubo, H. Murooka, Y. Kobayashi, T. Nishitoba, M. Shibuya, T. Yoneda, and T. Isoe. 2006. A c-fms tyrosine kinase inhibitor, Ki20227, suppresses osteoclast differentiation and osteolytic bone destruction in a bone metastasis model. *Mol. Cancer Ther*. 5:2634–2643.
28. Sudo, T., S. Nishikawa, M. Ogawa, H. Kataoka, N. Ohno, A. Izawa, S.I. Hayashi, and S.I. Nishikawa. 1995. Functional hierarchy of c-kit and c-fms in intramarrow production of CFU-M. *Oncogene*. 11:2469–2476.
29. Smith, L.E., E. Wesolowski, A. McLellan, S.K. Kostyk, R. D'Amato, R. Sullivan, and P.A. D'Amore. 1994. Oxygen-induced retinopathy in the mouse. *Invest. Ophthalmol. Vis. Sci*. 35:101–111.
30. Cai, J., and M. Boulton. 2002. The pathogenesis of diabetic retinopathy: old concepts and new questions. *Eye*. 16:242–260.
31. Baluk, P., T. Tammela, E. Ator, N. Lyubynska, M.G. Achen, D.J. Hicklin, M. Jeltsch, T.V. Petrova, B. Pytowski, S.A. Stacker, et al. 2005. Pathogenesis of persistent lymphatic vessel hyperplasia in chronic airway inflammation. *J. Clin. Invest*. 115:247–257.
32. Alitalo, K., T. Tammela, and T.V. Petrova. 2005. Lymphangiogenesis in development and human disease. *Nature*. 438:946–953.
33. Rutkowski, P., J. Kamińska, M. Kowalska, W. Ruka, and J. Steffen. 2003. Cytokine and cytokine receptor serum levels in adult bone sarcoma patients: correlations with local tumor extent and prognosis. *J. Surg. Oncol*. 84:151–159.

34. Murakami, M., Y. Zheng, M. Hirashima, T. Suda, Y. Morita, J. Ooehara, H. Ema, G.H. Fong, and M. Shibuya. 2008. VEGFR1 tyrosine kinase signaling promotes lymphangiogenesis as well as angiogenesis indirectly via macrophage recruitment. *Arterioscler. Thromb. Vasc. Biol.* 28:658–664.
35. Hiratsuka, S., Y. Maru, A. Okada, M. Seiki, T. Noda, and M. Shibuya. 2001. Involvement of Flt-1 tyrosine kinase (vascular endothelial growth factor receptor-1) in pathological angiogenesis. *Cancer Res.* 61:1207–1213.
36. Kerber, M., Y. Reiss, A. Wickersheim, M. Jugold, F. Kiessling, M. Heil, V. Tchaikovski, J. Waltenberger, M. Shibuya, K.H. Plate, and M.R. Machein. 2008. Flt-1 signaling in macrophages promotes glioma growth in vivo. *Cancer Res.* 68:7342–7351.
37. Shojaei, F., M. Singh, J.D. Thompson, and N. Ferrara. 2007. Tumor refractoriness to anti-VEGF treatment is mediated by CD11b+Gr1+ myeloid cells. *Nat. Biotechnol.* 25:911–920.
38. Roy, S., E. Cagliero, and M. Lorenzi. 1996. Fibronectin overexpression in retinal microvessels of patients with diabetes. *Invest. Ophthalmol. Vis. Sci.* 37:258–266.
39. Kerjaschki, D., N. Huttary, I. Raab, H. Regele, K. Bojarski-Nagy, G. Bartel, S.M. Kröber, H. Greinixm, A. Rosenmaier, F. Karlhofer, et al. 2006. Lymphatic endothelial progenitor cells contribute to de novo lymphangiogenesis in human renal transplants. *Nat. Med.* 12:230–234.
40. Kubota, Y., M. Hirashima, K. Kishi, C.L. Stewart, and T. Suda. 2008. Leukemia inhibitory factor regulates microvessel density by modulating oxygen-dependent VEGF expression in mice. *J. Clin. Invest.* 118:2393–2403.